Surface-induced phase transitions in ultrathin films of block copolymers

Dapeng Cao and Jianzhong Wu[a)]
Department of Chemical and Environmental Engineering, University of California, Riverside, California 92521

(Received 1 December 2004; accepted 1 March 2005; published online 13 May 2005)

We study theoretically the lamellar-disorder-lamellar phase transitions of *AB* diblock and tetrablock copolymers confined in symmetric slitlike pores where the planar surface discriminatingly adsorbs *A* segments but repels *B* segments, mimicking the hydrophobic/hydrophilic effects that have been recently utilized for the fabrication of environmentally responsive "smart" materials. The effects of film thickness, polymer volume fraction, and backbone structure on the surface morphology have been investigated using a polymer density-functional theory. The surface-induced phase transition is manifested itself in a discontinuous switch of microdomains or a jump in the surface density dictated by the competition of surface adsorption and self-aggregation of the block copolymers. The surface-induced first-order phase transition is starkly different from the thickness-induced symmetric-asymmetric or horizontal-vertical transitions in thin films of copolymer melts reported earlier. © *2005 American Institute of Physics*. [DOI: 10.1063/1.1897692]

I. INTRODUCTION

Thin films of block copolymers exhibit a wide variety of periodic microdomains that are potentially useful for photolithography or fabrication of nanoscopic devices. The morphology of these microdomains is controlled by the properties of block copolymers as well as the confining environment and external potentials such as electric fields,[1,2] temperature gradients,[3] graphoepitaxy,[4,5] chemically patterned substrates,[6–11] and the interfacial interactions.[12–15] For block copolymer melt confined between planar surfaces with a preference to one types of segments, previous theories,[16–19] simulations,[20–25] and experiments[26–28] indicate that microdomains of different blocks are formed parallel to the surface if the surface energy is sufficiently strong but perpendicular to the surface if the surface bias is removed or if the film thickness is incommensurable with the lamellar structure. The parallel to perpendicular phase transition of laminar or cylindrical microdomains in thin films of copolymers melts has been extensively studied over the past few decades.[12,18,28–30] In particular, a phenomenological free energy model proposed by Turner predicts the transitions among symmetric and asymmetric lamellar phases when the segments have a similar surface energy.[16] When the film is sufficiently thick or when the surface strongly adsorbs one of the blocks, however, only symmetric lamellar structures occur. Turner's theory has been extended to confined copolymers of other morphological structures and its predictions have been confirmed by more comprehensive self-consistent-mean-field calculations and experiments.[17]

In this work, we study the phase transitions and film morphology in confined block copolymers in which the lamellar microdomains of different segments can be switched by changing the degree of surface preference. Unlike most previous work that concerns with the phase transitions in thin films of copolymer melt induced by the chain incommensurability,[16,17] the focus here is on the effect of surface selectivity on the formation of ultrathin copolymer films at a fixed film thickness. Also different from previous work, the systems considered here are in contact with a bulk solution so that the amount of polymer within the film varies with surface energy and the polymer microstructure. We are interested in the effect of the polymer backbone structure, represented by multiblock copolymers, on the surface morphology at various discriminative surfaces.

II. MODEL DESCRIPTIONS

We consider an off-lattice mode of *AB* diblock and tetrablock copolymers confined between two planar walls where the surface attracts *A* segments but repels *B* segments. The block copolymers are represented by tangent chains of spherical *A* and *B* segments that have the same size but different energy. Each diblock copolymer consists of 25 *A* segments and 25 *B* segments and each tetrablock copolymer consists of 5*A*5*B*5*A*5*B*. The confined diblock and tetrablock copolymer systems mimic the thin films of amphiphilic block copolymers at a hydrophobic or hydrohilic substrate as investigated experimentally for tailoring the wettability of a substrate.[31,32]

The interaction between any two nonbonded polymer segments is described by a square-sell (SW) potential,

$$\varphi_{ij}(r)=\begin{cases}\infty, & r<\sigma\\ -\varepsilon_{ij}, & \sigma\leqslant r\leqslant\gamma\sigma\\ 0, & r>\gamma\sigma\end{cases}, \tag{1}$$

where σ is the segmental diameter; $\gamma\sigma$ is the square-well width ($\gamma=1.2$ is used throughout this work), and ε_{ij} is an energy parameter with the subscripts i and j indexing *A* or *B* segments. Beyond the hard-sphere collision, the pair interaction between like segments (*AA* or *BB*) is always attractive and that between unlike segments is always repulsive. The

[a)]Electronic mail: jwu@engr.ucr.edu

interaction energy between different type of segments is fixed at $\varepsilon^*_{AB}=\varepsilon^*_{BA}=-1.0$ where the negative sign indicates the repulsion, and the reduced energy is defined as $\varepsilon^*=\varepsilon/kT$. To mimic the behavior of hydrophobic effects, we assume that the attraction between *AA* segments is $\varepsilon^*_{AA}=3.0$ substantially stronger than that between *BB* segments ($\varepsilon^*_{BB}=1.0$). The segment-wall interaction is also represented by the SW potential with the well width equal to the segmental radius.

All systems considered in this work are in the strong segregation limit, i.e., $\chi M \gg 20$ where M is the number of segments and χ is the Flory parameter estimated from $3(\varepsilon^*_{AA}+\varepsilon^*_{BB}-2\varepsilon^*_{AB})$ as in a standard polymer lattice model assuming the coordinate number is 6. We expect that micellar, lamellar, or other mesoscopic phases may form in the bulk phase that is in equilibrium with the thin film. However, because the focus of this work is on the structure and phase transition of the confined copolymers, for convenience, the chemical potential of a copolymer is mapped into a bulk volume fraction assuming that the copolymers would be in a disordered state.

III. DENSITY FUNCTIONAL THEORY

The copolymer films confined between two surfaces are directly in contact with a bulk solution, i.e., they are specified in terms of temperature, volume, chemical potential, and the interactions between the polymer segments and the confining surfaces. The microstructure and thermodynamic properties of the model system can be represented by a recently developed polymer density-functional theory (PDFT).[33,34] Specifically, the Helmholtz energy functional of a polymeric system can be expressed in terms of that corresponding to a system of ideal chains at system temperature and chemical potential where all nonbonded interactions are turned off, and an excess part due to nonbonded intermolecular and intramolecular interactions

$$F[\rho_M(\mathbf{R})] = F_{\mathrm{id}}[\rho_M(\mathbf{R})] + F_{\mathrm{ex}}[\rho_M(\mathbf{R})], \tag{2}$$

where $\mathbf{R}$ is a composite vector $(\mathbf{r}_1,\mathbf{r}_2,\ldots,\mathbf{r}_M)$ representing the positions of individual segments, and $\rho_M(\mathbf{R})$ stands for a multidimensional density profile. The Helmholtz energy functional of ideal chains is known exactly,

$$\beta F_{\mathrm{id}}[\rho_M(\mathbf{R})] = \int d\mathbf{R}\rho_M(\mathbf{R})[\ln \rho_M(\mathbf{R}) - 1] + \beta \int d\mathbf{R}\rho_M(\mathbf{R})V_{\mathrm{bond}}(\mathbf{R}). \tag{3}$$

Here $V_{\mathrm{bond}}(\mathbf{R})$ specifies the bond potential which is related to the Dirac-δ function

$$\exp[-\beta V_{\mathrm{bond}}(\mathbf{R})] = \prod_{i=1}^{M-1} \frac{\delta(|\mathbf{r}_{i+1}-\mathbf{r}_i|-\sigma)}{4\pi\sigma^2}, \tag{4}$$

where M denotes the number of segments for each molecule, and $\mathbf{r}$ denotes a segmental position. In Eqs. (3) and (4), $\beta=(kT)^{-1}$ with k standing for the Boltzmann constant and T for temperature. Because Eq. (3) is true for an arbitrary bond potential, the DFT described here is able to take into account the chemical details of a polymeric system at least in principle.

The key assumption in the polymer density functional theory is that the excess Helmholtz energy functional is exclusively determined by the density profiles of individual segments and the details of bond connectivity. In other words, for a given configuration of molecules represent by the composite vector $\mathbf{R}$, the excess Helmholtz energy is not directly related to the bond potential. Therefore, in terms of the excess Helmholtz energy functional, the reference system is a monomeric fluid with the same segmental density distributions. For the block copolymers considered in this work, the nonbonded intersegmental interaction consists of two parts: one is the hard-sphere repulsion and the other is van der Waals attraction. Correspondingly, the excess Helmholtz energy functional can be formally written as[34]

$$F_{\mathrm{ex}}[\rho_A(\mathbf{r}),\rho_B(\mathbf{r})] = F_{\mathrm{hs}} + F_{\mathrm{att}} + F_{\mathrm{chain}}, \tag{5}$$

where $\rho_A(\mathbf{r})$ and $\rho_B(\mathbf{r})$ are the density profiles of segments *A* and *B*. The first two terms on the right-hand side of Eq. (5) represent the excess Helmholtz energies due to the hard-sphere repulsion and van der Waals attraction, respectively. These two terms depend only on the segmental densities. Conversely, F_{chain} takes into account the effect of chain connectivity on the correlation between segments that, in the framework of the thermodynamic perturbation theory, can be related to the segmental densities and the backbone structure (but not the bond potential).

Following our previous work,[35,36] the hard-sphere part of the Helmholtz energy functional is represented by a modified fundamental measure theory,[37]

$$\beta F_{\mathrm{hs}} = \int d\mathbf{r}\left[-n_0\ln(1-n_3) + \frac{n_1n_2-\mathbf{n}_{V1}\cdot\mathbf{n}_{V2}}{1-n_3} + (n_2^3/3 - n_2\mathbf{n}_{V2}\cdot\mathbf{n}_{V2})\left(\frac{\ln(1-n_3)}{12\pi n_3^2} + \frac{1}{12\pi n_3(1-n_3)^2}\right)\right], \tag{6}$$

where $n_\alpha(\mathbf{r})$, $\alpha=0$, 1, 2, 3, *V*1, *V*2 are weighted densities defined by Rosenfeld,[38]

$$n_\alpha(\mathbf{r}) = \sum_j n_{\alpha j}(\mathbf{r}) = \sum_j \int \rho_j(\mathbf{r}')\omega_j^\alpha(\mathbf{r}-\mathbf{r}')d\mathbf{r}', \tag{7}$$

where ϖ_j^α ($\alpha=0,1,2,3,V1,V2$) are six weight functions, and the subscript $j=1$, 2 denote the index of segments *A* and *B*. Three of the six weight functions are defined as[38]

$$\omega_j^2(r) = \delta(\sigma/2-r), \quad \omega_j^3(r) = \Theta(\sigma/2-r), \quad \boldsymbol{\omega}_j^{V2}(\mathbf{r}) = (\mathbf{r}/r)\delta(\sigma/2-r), \tag{8}$$

where $\Theta(r)$ stands for the Heaviside step function, $\delta(r)$ for the Dirac-δ function. $\omega_j^2(r)$ and $\omega_j^3(r)$ are directly related to the particle surface area and volume, respectively. In Eq. (8), $\boldsymbol{\omega}_j^{V2}(\mathbf{r})$ denotes the gradient across a sphere in the $\mathbf{r}$ direction. The other weight functions are proportional to those given in Eq. (8)

$$\omega_j^0(r) = \omega_j^2(r)/(\pi\sigma^2), \quad \omega_j^1(r) = \omega_j^2(r)/(2\pi\sigma),$$
$$\boldsymbol{\omega}_j^{V1}(\mathbf{r}) = \boldsymbol{\omega}_j^{V2}(\mathbf{r})/(2\pi\sigma). \tag{9}$$

A salient feature of the fundamental measure theory is that all weight functions are independent of the density profiles.

The excess Helmholtz energy functional due to the chain connectivity is given by a generalized first-order perturbation theory,[36]

$$\beta F_{\text{chain}} = \int d\mathbf{r} \frac{1-M}{M} n_0 \xi \ln y^{\text{hs}}(\sigma, n_\alpha), \tag{10}$$

where $\xi = 1 - \mathbf{n}_{V_2} \cdot \mathbf{n}_{V_2} / n_2^2$ is defined as an inhomogeneous factor and $y^{\text{hs}}(\sigma, n_\alpha)$ is the contact value of the cavity correlation function between segments,

$$y^{\text{hs}}(\sigma, n_\alpha) = \frac{1}{1-n_3} + \frac{n_2 \xi \sigma}{4(1-n_3)^2} + \frac{n_2^2 \xi \sigma}{72(1-n_3)^3}. \tag{11}$$

Equation (10) is not directly related to the bonding potentials of polymeric molecules that have been already included in Eq. (3). Instead, this term takes into account the effect of chain connectivity on the correlation between nonbonded polymeric segments. If the density profiles are everywhere uniform, Eqs. (10) and (11) reduces to the first-order thermodynamic perturbation theory of bulk fluids.[39,40]

Finally, the excess Helmholtz energy functional due to van der Waals attractions $\beta F_{\text{ex}}^{\text{att}}$ is represented by a mean-field approximation,

$$\beta F_{\text{ex}}^{\text{att}} = \tfrac{1}{2} \int \int d\mathbf{r}\, d\mathbf{r}' \sum_{i,j=A,B} \rho_i(\mathbf{r}) \rho_j(\mathbf{r}) \beta \varphi_{ij}^{\text{att}}(|\mathbf{r} - \mathbf{r}'|), \tag{12}$$

where $\varphi_{ij}^{\text{att}}(r)$ is described in Eq. (1). We have shown that the mean-field approximation is quantitatively accurate for polymers near attractive walls.[33]

At equilibrium, the molecular density profile $\rho_M(\mathbf{R})$ can be solved by minimizing the grand potential

$$\Omega[\rho_M(\mathbf{R})] = F[\rho_M(\mathbf{R})] + \int [\psi_M(\mathbf{R}) - \mu_M] \rho_M(\mathbf{R}) d\mathbf{R}, \tag{13}$$

where μ_M is the chemical potential of the copolymer chain. As mentioned earlier, the chemical potential can be mapped into a bulk density assuming the system is in a disordered state,[33]

$$\beta\mu_M = \ln \rho_M + M\beta\mu_M^{\text{hs,bulk}}(\rho_{\text{bulk}}) + (1-M) \times \left[\ln y^{\text{hs,bulk}}(\sigma) + \rho_{\text{bulk}} \frac{\partial \ln y^{\text{hs,bulk}}(\sigma)}{\partial \rho_{\text{bulk}}} \right] + \sum_{\substack{i \in A \text{ or } B \\ j \in A \text{ or } B}} (-4\pi/3)(\lambda^3 - 1) \varepsilon_{ij}^* \rho_{\text{bulk}} x_i x_j \sigma^3, \tag{14}$$

where $\rho_{\text{bulk}} = M\rho_M$ is the total bulk density of segments A and B, and $\mu^{\text{hs,bulk}}$ is the excess chemical potential due to hard-sphere interactions represented by the Carnahan–Starling equation of state, x_i (or x_j) is the molar fraction of segment i (or j) where i (or j) denotes the index of segments A or B. In Eq. (14), $\psi_M(\mathbf{R})$ is the external potential for individual segments.

According to the variational principle, the stationary condition of the grand potential satisfies

$$\frac{\delta\Omega[\rho_M(\mathbf{R})]}{\delta\rho_M(\mathbf{R})} = 0. \tag{15}$$

Once we have the molecular density profile $\rho_M(\mathbf{R})$, the segmental densities are calculated from

$$\rho_{A \text{ or } B}(\mathbf{r}) = \sum_{j \in A \text{ or } B} \rho_{sj}(\mathbf{r}) = \sum_{j \in A \text{ or } B} \int d\mathbf{R}\, \delta(\mathbf{r} - \mathbf{r}_j) \rho_M(\mathbf{R}). \tag{16}$$

Substitution of Eq. (2) and (13) into Eq. (15) yields the Euler–Lagrange equation

$$\rho_M(\mathbf{R}) = \exp[\beta\mu_M - \beta V_{\text{bond}}(\mathbf{R}) - \beta \sum_{j \in A} \lambda_A(\mathbf{r}_j) - \beta \sum_{k \in B} \lambda_B(\mathbf{r}_k)], \tag{17}$$

where $\rho_j(\mathbf{r})$ stands for the local density of segment j; the self-consistent field λ is related to the excess Helmholtz energy functional F_{ex} and the external potential for individual segments φ_A and φ_B:

$$\lambda_A(\mathbf{r}_j) = \frac{\delta F_{\text{ex}}}{\delta \rho_A(\mathbf{r}_j)} + \varphi_A(\mathbf{r}_j), \quad \lambda_B(\mathbf{r}_k) = \frac{\delta F_{\text{ex}}}{\delta \rho_B(\mathbf{r}_k)} + \varphi_B(\mathbf{r}_k). \tag{18}$$

Combining Eqs. (16) and (17), we have a set of coupled integral equations for the segmental density profiles,

$$\rho_{si}(\mathbf{r}) = \int d\mathbf{R}\, \delta(\mathbf{r} - \mathbf{r}_i) \exp[\beta\mu_M - \beta V_{\text{bond}}(\mathbf{R}) - \beta \sum_{j \in A} \lambda_A(\mathbf{r}_j) - \beta \sum_{k \in B} \lambda_B(\mathbf{r}_k)]. \tag{19}$$

With the assumption that the density distribution varies only in the direction perpendicular to the surface (z), i.e., $\rho_{sl}(\mathbf{r}) = \rho_i(z)$, the average segmental densities are given by

$$\rho_{A \text{ or } B}(z) = \exp(\beta\mu_M) \sum_{i \in A \text{ or } B} G_L^i(z) \exp[-\beta\lambda_i(z)] G_R^i(z), \tag{20}$$

where $G_L^i(z)$ and $G_R^i(z)$, respectively, are the left and right recurrence functions,

$$G_L^i(z) = \frac{1}{2\sigma} \int_{z-\sigma}^{z+\sigma} \exp[-\beta\lambda_{i-1}(z)] G_L^{i-1}(z) dz, \tag{21}$$

$$G_R^i(z) = \frac{1}{2\sigma} \int_{z-\sigma}^{z+\sigma} \exp[-\beta\lambda_{i+1}(z)] G_R^{i+1}(z) dz \tag{22}$$

with $G_L^i(z) = 1$ and $G_R^M(z) = 1$, and $i = 1, 2, \ldots, M$. Equation (20) can be solved using the Picard iteration method.[33] Because the Boltzmann factors $\exp[-\beta\lambda_i(z)]$ depend on the

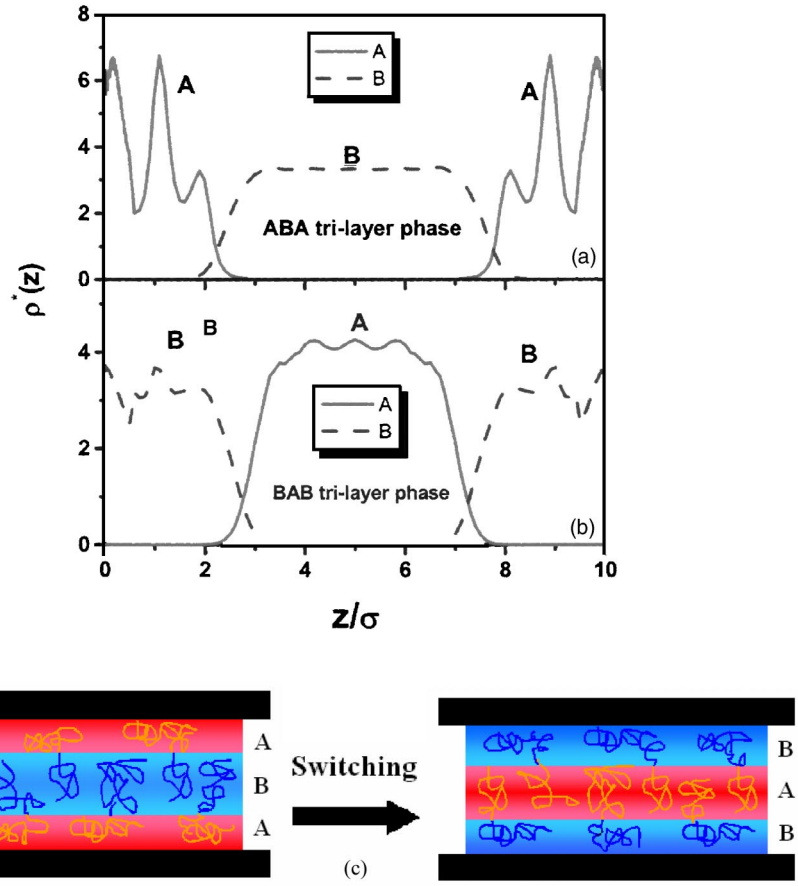

FIG. 1. The structures of diblock copolymer films in the pore of $H^*=10$ at the bulk packing fraction $\phi_b=0.2$. (a) *ABA* trilayer films at wall potential $\varepsilon_W^*=0.5$; (b) *BAB* trilayer films formed at wall potential $\varepsilon_W^*=0.3$; (c) sketches of microphase-separated domain switching from *ABA* to *BAB* phase.

identity of the segment *A* or *B*,[33,34] the left and right recurrence functions bear no symmetry.

IV. RESULTS AND DISCUSSION

As mentioned earlier, the systems considered in this work are rather different from previous theoretical investigations on the thin films of copolymer melts where the total number of polymers and volume are fixed. Instead, here the polymers are in direct equilibrium with a bulk phase so that the amount of polymer within a slitlike pore is determined by the surface energy as well as polymer configuration. As a result, the copolymers are less likely to be "frustrated," i.e., the formation of asymmetric or perpendicular lamellar structures within the slit pore is not favored by neither energetic nor entropic effects. With these considerations we assume that the segmental density profile is always symmetric and it varies only in the direction perpendicular to the surface.

We consider first the segment distributions of a diblock copolymer consisting of 25 *A* segments and 25 *B* segments ($A_{25}B_{25}$) confined between planar surfaces of different preferential energies. Following a phenomenological analysis,[17] we estimate the lamellar period of the block copolymers in the bulk phase:

$$L_0/\sigma = 2\left(\frac{1}{3}\sqrt{\frac{\chi}{6}}\right)^{1/3} M^{2/3} \approx 23. \tag{23}$$

If the copolymers are in a thick film (on the order of L_0) confined between substrates preferentially adsorb *A* segments, previous investigations based on a phenomenological free energy and the self-consistent field theory conclude that the confinement leads to no significant stretching or compression of the lamellar layers. However, in an ultrathin film, the lamellar period is determined primarily by the film thickness.

Figure 1 depicts the calculated density profiles of *A* and *B* segments in a slitlike pore at two different surface energies. When the surface shows preferential attraction of *A* segments but repulsion of *B* segments, we find *ABA* trilayer morphology parallel to the surface [Fig. 1(a)] similar to that observed in experiments.[27] The widths of the different layers indicate that essentially only *A* segments are in direct contact with the surface and all *B* segments are accumulated in the middle layer. The widths of the *A* and *B* parallel layers suggest that the *A* and *B* blocks are at different levels of extension, i.e., the *B* block is slightly more stretched than the *A* block. At a slightly lower surface energy ($\varepsilon_W^*=0.3$), similar parallel microdomains are also observed but in this case, the microdomains of *A* and *B* segments switch positions, yielding a *BAB* trilayer [Fig. 1(b)]. Even though the direct contact between the surface and *B* segments is energetically unfavorable, the confinement increases the probability of association among *A* segments and thus significant amount of polymers are still adsorbed in the pore. Figure 1(c) depicts the two different states of copolymer film schematically. Unlike the symmetric-asymmetric lamellar transition induced by the film thickness, the switch of the *ABA* and *BAB* trilayer films is dictated by the competition between surface-driven adsorption and self-association of *A* segments.

To exam the effect of copolymer backbone structure on

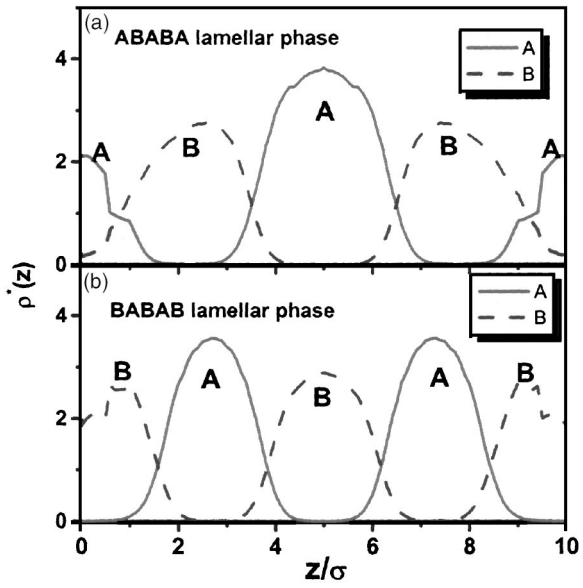

FIG. 2. The microstructure of tetrablock copolymer films formed in the pore at bulk packing fraction $\phi_b=0.2$. (a) *ABABA* lamellar films formed at wall potential $\varepsilon_W^*=0.5$ (top panel); (b) *BABAB* lamellar films formed at wall potential $\varepsilon_W^*=0.3$ (bottom panel).

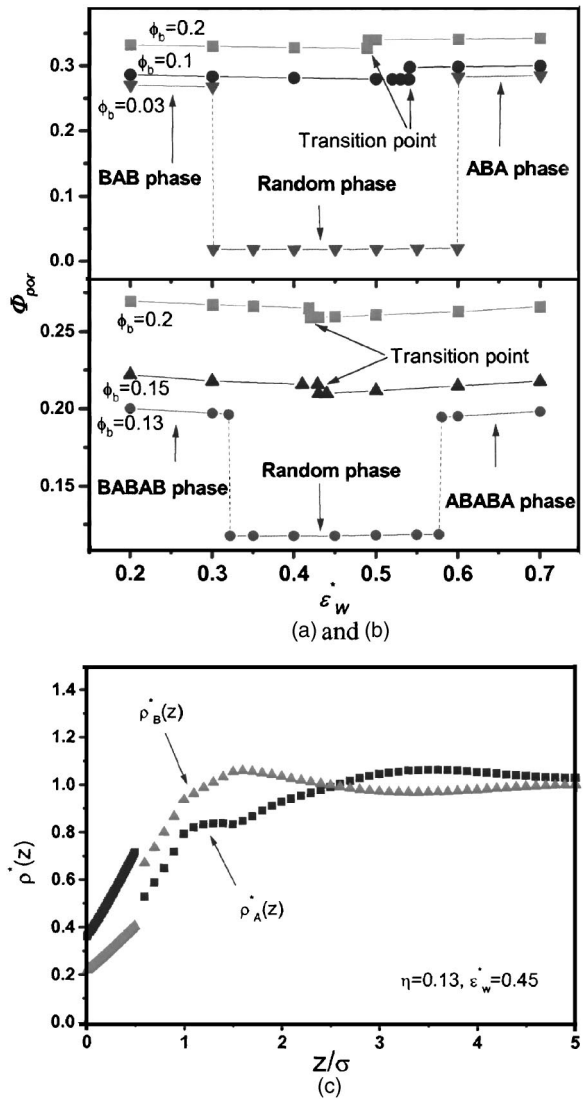

FIG. 3. The average volume fraction of the copolymers in the pore vs wall potential. (a) Diblock copolymers (top panel); (b) tetrablock copolymers (bottom panel); (c) microstructure of the confined tetrablock copolymers in the random phase.

the thin-film morphology, we present in Fig. 2 the microstructures of a tetrablock copolymer $A_5B_5A_5B_5$ consisting of alternating five *A* segments and five *B* segments. As for diblock copolymers, two types of lamellar morphology are observed, one corresponding to strongly discriminating surfaces and the other corresponding to weakly discriminating surfaces. For the tetrablock copolymers, an *ABABA* or *BABAB* five-layer lamellar film is formed due to the increase of the number of blocks, suggesting that the number of layers can be effectively controlled by the backbone structure. For both strongly and weakly discriminating surfaces, the surface layer is relatively thinner and less dense than the middle layers because in this case, the polymer contour length is smaller than the pore width and the copolymer chains are approximately aligned normal to the surface.

The lamellar-lamellar transition of confined block copolymers can be easily identified by a discontinuous jump in the adsorption isotherm. Figure 3(a) shows the average volume fraction of the $A_{25}B_{25}$ diblock copolymer in the slit pore as a function of the wall potential with the fixed interaction energies among polymeric segments at three bulk packing fractions. When the wall potential is weak, *BAB*-type lamellar structures are formed and the surface layers are rich in energetically unfavorable *B* segments. At the point of lamellar-lamellar transition (the point is denoted by arrows in Fig. 3), the adsorption isotherm presents a discontinuity as appeared in a typical first-order prewetting phase transition. Figure 3(a) shows that with the same surface energy, the average volume fraction of the *ABA* trilayer structure is slightly greater than that of the *BAB* trilayer structure. This may be explained by the favorable interactions between the surface and *A* segments. Figure 3(b) shows that for $A_5B_5A_5B_5$ tetrablock copolymers, the switch of microdomains from the *BABAB* to *ABABA* films leads to a decrease in the average volume fraction. A comparison of Figs. 3(a) and 3(b) reveals that the total amount of adsorption depends not only on the surface energy but also on the commensurability of the pore size and the backbone structure. The alternating structure of the tetrablock copolymer causes more configurational restriction so that the polymer volume fraction of *BABAB* phase in the transition point is greater than that of *ABABA* phase. At low concentration of block copolymers, a random phase appears between the *ABA* and *BAB* lamellar phases. Apparently, the microstructure in the random phase as depicted in Fig. 3(c) is different from those in lamellar phases. In this case, the segmental density approaches to the bulk density.

The symmetric lamellar-lamellar transition induced by the surface energy is different from the thickness-induced symmetric-asymmetric transition occurred in a polymer melt. For the "symmetric-asymmetric" transitions in thin films of copolymer melts reported in previous theoretical investigations,[16] the amount of polymer within the pore is fixed and the phase transition is introduced by a competition

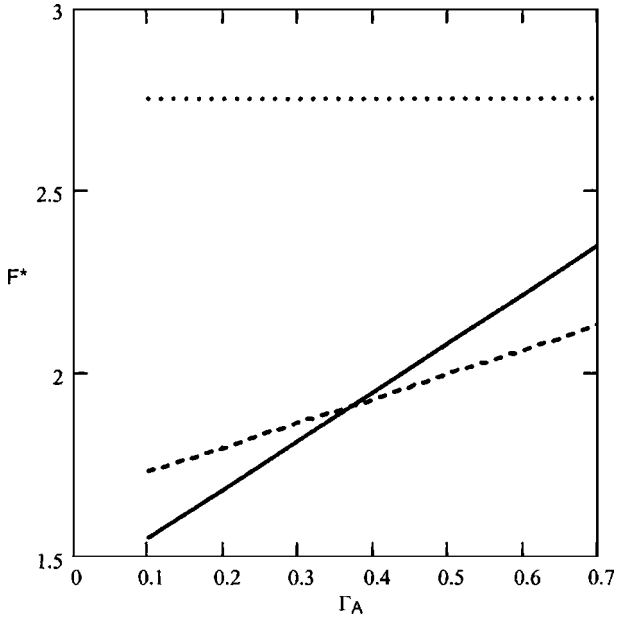

FIG. 4. The Helmholtz energy per polymer (in units of that in the bulk) as a function of $\Gamma_A = \gamma_{AS}/\gamma_{AB}$, the ratio of *A* surface and *A*-*B* surface tensions, according to a phenomenological model by Turner. The solid line represents that for a symmetric lamellar layer (*ABBA*) where both surfaces are covered by the *A* segments, the dashed line represents that for an asymmetric lamellar (*AB*) where the *A* segments are in contact with one surface and the *B* segments are in contact with the other, and the dotted line is for a symmetric *BAAB* lamellar where both surfaces are in contact with the *B* segments. Here the film thickness is fixed at $H = L_0/2$ and $\Gamma_B = \gamma_{BS}/\gamma_{AB} = 1$, with the assumption that the surface preferably adsorbs *A* segments but repels *B* segment.

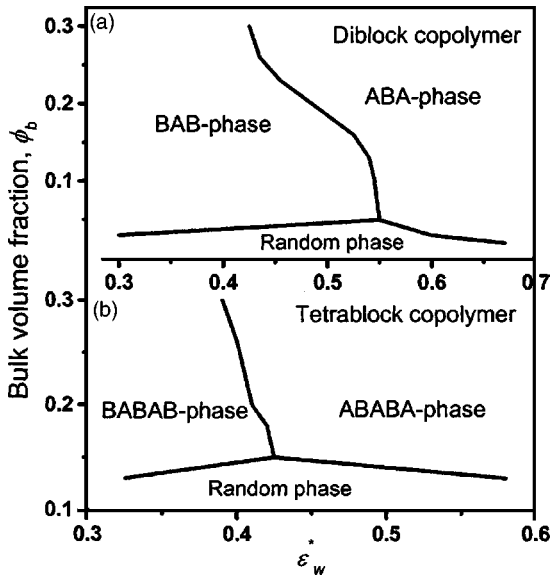

FIG. 5. Phase diagrams of the copolymer lamellar films in the slit pore of $H^* = 10$. (a) Diblock copolymer (top panel); (b) tetrablock copolymer (bottom panel).

between the chain elasticity and surface energy. For an incompressible system at a film thickness similar to the case considered in this work, the phenomenological free energy model by Turner[16] predicts that a symmetric *ABBA* lamellar structure is favored when the interfacial tension between the *A* domain and the substrate is small but an asymmetric *AB* lamellar is favored as the substrate- *A* interfacial tension increases. Conversely, the *BAAB* lamellar always has a free energy higher than that of the *ABBA* and *AB* structures. As a result, the symmetry *BAAB* structure will not appear in an incompressible case. To illustrate, Fig. 4 depicts how the free energies of different surface morphology vary with the surface energy of *A* segments if the system is incompressible. When there is a strong attraction between the surface and *A* segments as considered in this work, the reduced interfacial tension $\Gamma_A = \gamma_{AS}/\gamma_{AB}$ is small and the *ABBA* morphology is thermodynamically favored. However, as Γ_A increases the *AB* morphology becomes thermodynamically more stable. Indeed, for an incompressible system, the surface-induced *ABBA* to *AB* transition is rather similar to the thickness-induced transition.

For compressible systems discussed in this work, the phase transitions rather resemble the prewetting transition for the adsorption of polymers near a surface. This similarity is more evident by considering the discontinuity of the average polymer volume fraction within the pore as the surface energy is increased. However, different from a normal prewetting transition though, the transition between *ABBA* and *BAAB* structures involves little change in the total amount of adsorption and at low bulk densities, the transition involves a big change in average polymer concentration within the pore, rather similar to a vapor-liquid capillarity condensation. Besides, there is a reentrance transition as the surface energy grows continuously. In general, the prewetting transition could be coupled with a capillary condensation within the pore but depending on the pore size and surface energy, it could also exist outside of the miscibility gap. Detailed examination of the interplay between the layering transitions and demixing will be explored in a future work.

Figure 5 depicts the lamellar-random-lamellar phase transitions in the diblock (a) and tetrablock (b) copolymers at a fixed film thickness. For diblock copolymers [Fig. 5(a)], the top-right zone is the *ABA* phase when the surfaces are in contact with the energetically favorable segments; the top-left zone is the *BAB* phase, and the bottom zone is a random phase. Figure 5(a) indicates that the lamellar phase appears only beyond a critical bulk volume fraction, i.e., it must be greater than 0.05 for the diblock copolymers considered here. Once the bulk volume fraction in the pore is smaller than the critical value, a random phase starts to appear. Figure 5(b) shows a similar phase diagram for the tetrablock copolymer. Noticeably, the critical volume fraction is sensitive to the backbone structure. For the tetrablock copolymer, the lamellar phase appears when the average volume fraction in the pore exceeds 0.15.

To investigate the effect film thickness on the lamellar-lamellar phase transition of block copolymers, we present in Fig. 6 the critical wall potential at the onset of lamellar-lamellar phase transition for thin films of three different thicknesses. For $H^* \equiv H/\sigma = 6$, the critical wall potential is relatively insensitive to the bulk density. However, for $H^* = 10$, and 16, the critical wall potential sharply declines with the bulk packing fraction due to a collective effect. At low bulk density, a stronger interfacial energy is required to overcome the entropic barrier that disfavors the adsorption of polymeric molecules. For tetrablock copolymers, a trilayer

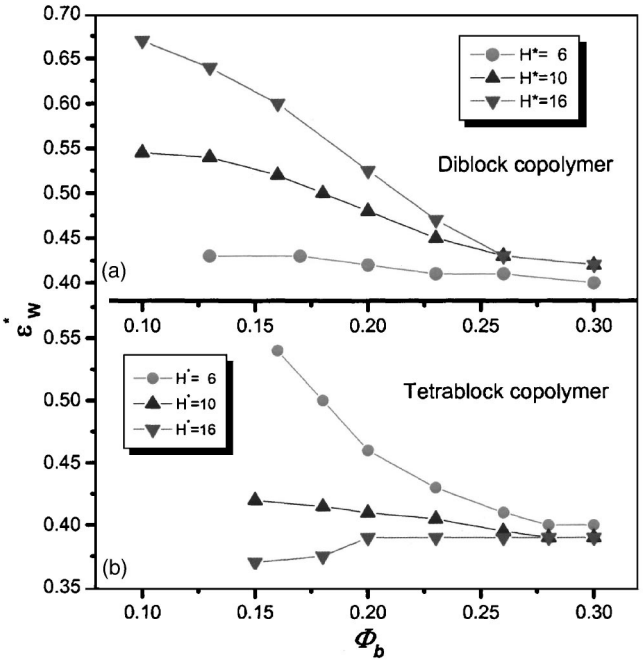

FIG. 6. The dependence of the wall potential corresponding to lamellar-lamellar transition on bulk packing fraction at different pore widths. (a) Diblock copolymer (top panel); (b) tetrablock copolymer (bottom panel).

films is formed for the pore of $H^*=6$ and a seven-layer film is formed for the pore $H^*=16$. While the lamellar-lamellar phase transition can still be observed for the tetrablock copolymers, the dependence of the critical wall potential on the bulk packing fraction is entirely different from that for diblock copolymers. For a large pore ($H^*=16$), the critical wall potential increases with the bulk density and the opposite is observed for smaller pores. Surprisingly, the critical wall potential at the microdomain switch is sensitive to the bulk density as the pore size is close to the length of one block of the copolymer, while it becomes insensitive when the pore width significantly deviates from the contour length of each block.

V. CONCLUSIONS

We have theoretically investigated the formation of different lamellar phases in block copolymer thin films at equilibrium with a bulk solution. The phase transitions occurred in these compressible systems are rather different from the thickness-induced transitions in the thin films of copolymer melt reported earlier.[16,17] Here the phase transitions is mainly due to the competition between the self-aggregation and surface adsorption rather the film thickness incommensurability. However, there are some similarities between the "lamellar-disorder-lamellar" transitions and prewetting except that here the phase behavior is much richer due to the structure formation of block copolymers. The energy-induced transitions are manifested in either a discontinuous switch of microdomains or a jump in the surface density. The effects of polymer backbone structure and film thickness on the phase behavior of thin films have also been investigated. As shown in recent experiment,[32] the change of wall potential may be achieved by varying the humidity of hydrophilic/hydrophobic interfaces under the stimuli of an environmental temperature. The lamellar-lamellar transition could find applications in the fabrication of the environmentally responsive biosensors.[41,42]

ACKNOWLEDGMENTS

The authors are grateful to Professor Zhen-Gang Wang at Caltech for insightful comments and useful discussions. This work was supported by the National Science Foundation under Grant No. CTS-0406100.

[1] T. L. Morkved, M. Lu, A. M. Urbas, E. E. Ehrichs, H. M. Jaeger, P. Mansky, and T. P. Russell, Science **273**, 931 (1996).
[2] A. Boker, H. Elbs, H. Hansel, A. Knoll, S. Ludwigs, H. Zettl, V. Urban, V. Abetz, A. H. E. Muller, and G. Krausch, Phys. Rev. Lett. **89**, 135502 (2002).
[3] P. R. van der Meer, G. C. M. Meijer, M. J. Vellekoop, H. M. M. Kerkvliet, and T. J. J. van den Boom, Sens. Actuators, A **A71**, 27 (1998).
[4] S. O. Kim, H. H. Solak, M. P. Stoykovich, N. J. Ferrier, J. J. de Pablo, and P. F. Nealey, Nature (London) **424**, 411 (2003).
[5] R. D. Peters, X. M. Yang, Q. Wang, J. J. de Pablo, and P. F. Nealey, J. Vac. Sci. Technol. B **18**, 3530 (2000).
[6] C. Harrison, D. H. Adamson, Z. D. Cheng, J. M. Sebastian, S. Sethuraman, D. A. Huse, R. A. Register, and P. M. Chaikin, Science **290**, 1558 (2000).
[7] L. Ionov, S. Minko, M. Stamm, J. F. Gohy, R. Jerome, and A. Scholl, J. Am. Chem. Soc. **125**, 8302 (2003).
[8] M. J. Fasolka, D. J. Harris, A. M. Mayes, M. Yoon, and S. G. J. Mochrie, Phys. Rev. Lett. **79**, 3018 (1997).
[9] M. Wolff, U. Scholz, R. Hock, A. Magerl, V. Leiner, and H. Zabel, Phys. Rev. Lett. **92**, 255501 (2004).
[10] Y. Tsori and D. Andelman, Macromolecules **34**, 2719 (2001).
[11] G. G. Pereira and D. R. M. Williams, Phys. Rev. Lett. **80**, 2849 (1998).
[12] G. J. Kellogg, D. G. Walton, A. M. Mayes, P. Lambooy, T. P. Russell, P. D. Gallagher, and S. K. Satija, Phys. Rev. Lett. **76**, 2503 (1996).
[13] I. Luzinov, S. Minko, and V. V. Tsukruk, Prog. Colloid Polym. Sci. **29**, 635 (2004).
[14] P. Mansky, T. P. Russell, C. J. Hawker, J. Mays, D. C. Cook, and S. K. Satija, Phys. Rev. Lett. **79**, 237 (1997).
[15] R. D. Peters, X. M. Yang, and P. F. Nealey, Macromolecules **35**, 1822 (2002).
[16] M. S. Turner, Phys. Rev. Lett. **69**, 1788 (1992).
[17] D. G. Walton, G. J. Kellogg, A. M. Mayes, P. Lambooy, and T. P. Russell, Macromolecules **27**, 6225 (1994).
[18] T. P. Russell, Curr. Opin. Colloid Interface Sci. **1**, 107 (1996).
[19] A. L. Frischknecht, J. G. Curro, and L. J. D. Frink, J. Chem. Phys. **117**, 10398 (2002).
[20] Q. Wang, Q. L. Yan, P. F. Nealey, and J. J. de Pablo, J. Chem. Phys. **112**, 450 (2000).
[21] Q. Wang, Q. L. Yan, P. F. Nealey, and J. J. de Pablo, Macromolecules **33**, 4512 (2000).
[22] Q. Wang, S. K. Nath, M. D. Graham., P. F. Nealey, and J. J. de Pablo, J. Chem. Phys. **112**, 9996 (2000).
[23] Q. Wang, P. F. Nealey, and J. J. de Pablo, Macromolecules **34**, 3458 (2001).
[24] Q. Wang, P. F. Nealey, and J. J. de Pablo, Macromolecules **35**, 9563 (2002).
[25] Q. Wang, P. F. Nealey, and J. J. de Pablo, Macromolecules **36**, 1731 (2003).
[26] E. Huang, T. P. Russell, C. Harrison, P. M. Chaikin, R. A. Register, C. J. Hawker, and J. Mays, Macromolecules **31**, 7641 (1998).
[27] S. H. Anastasiadis, T. P. Russell, S. K. Satija, and C. F. Majkrzak, Phys. Rev. Lett. **62**, 1852 (1989).
[28] E. Huang, L. Rockford, T. P. Russell, and C. J. Hawker, Nature (London) **395**, 757 (1998).
[29] Y. Tsori and D. Andelman, Macromolecules **36**, 8560 (2003).
[30] R. A. Register, Nature (London) **424**, 378 (2003).
[31] D. C. Popescu, N. A. A. Rossi, C. T. Yeoh, G. G. Durand, D. Wouters, P. Leclere, P. Thune, S. J. Holder, and N. Sommerdijk, Macromolecules **37**, 3431 (2004).
[32] S. H. Anastasiadis, H. Retsos, S. Pispas, N. Hadjichristidis, and S. Neophytides, Macromolecules **36**, 1994 (2003).

[33]D. P. Cao and J. Z. Wu, Macromolecules **38**, 971 (2005).
[34]D. P. Cao and J. Z. Wu, J. Chem. Phys. **121**, 4210 (2004).
[35]Y. X. Yu and J. Z. Wu, J. Chem. Phys. **118**, 3835 (2003).
[36]Y. X. Yu and J. Z. Wu, J. Chem. Phys. **117**, 2368 (2002).
[37]Y. X. Yu and J. Z. Wu, J. Chem. Phys. **117**, 10156 (2002).
[38]Y. Rosenfeld, J. Phys.: Condens. Matter **14**, 9141 (2002).
[39]D. Chandler and L. R. Pratt, J. Chem. Phys. **65**, 2925 (1976).
[40]M. S. Wertheim, J. Stat. Phys. **35**, 19 (1984).
[41]J. T. Koberstein, J. Polym. Sci., Part B: Polym. Phys. **42**, 2942 (2004).
[42]T. P. Russell, Science **297**, 964 (2002).